International Journal of Applied Engineering Research ISSN 0973-4562 Volume 13, Number 8 (2018) pp. 6183-6187

The Study of Abdominal Aortic Aneurysm Rupture Risk using Fluid-Structure Interaction

Taewon Seo*†, Guek-don Shin* and Do-Il Kim**

**Department of Mechanical and Automotive Engineering, Andong National University, Andong, 36729, Korea.*

***CEO, Water Pipe CO LTD, Andong, 36656, Korea.*

†Corresponding author

Abstract

The aims of mathematical modeling of aneurysm in this study are to lead the understanding of pathogenesis of the disease and to improve the criteria for the prediction of rupture risk. Therefore in this study, FSI simulations were performed to investigate the effect of neck angular variation on the rupture risk of AAA. As the neck angulation increases, it can be seen the region of the lateral side along the proximal axis is gathering more and more blood flow while the opposite region is gradually decreasing the flow to form a large vortex. Wall displacement was higher and longer as the neck angulation is larger, and this can effect on AAA, moreover, could collapse it. We also found that as the neck angulation increases, the Von Mises stress increases and the possibility of rupture increases. In particular, the Von Mises stress at point A in the proximal site is the highest and the possibility of rupture is predicted here.

***Keywords*:** Abdominal Aortic Aneurysm, Rupture Risk, Fluid-Structure Interaction, Neck Angulation, Wall Shear Stress

INTRODUCTION

The abdominal aortic aneurysm (AAA) is a balloon-shaped vascular enlargement in the abdominal aortic blood vessels arising from the subclavian aorta, which is the lower part of the abdominal aorta[1,2]. The prevalence of this disease is known to be 6~8% in men over 65 years old and more than 10% in men over 80 years old.

If an aneurysm grows more than 1 cm per year or is more than 5.5 cm in size, it is known to treat an abdominal aneurysm using intervention[3-5]. Currently, interventional methods are Open Surgical Repair (OSR) and Endo-Vascular Aortic Repair (EVAR). OSR is performed by cutting the lesion of the AAA using cylindrical tube called a graft, while EVAR is a method of pushing the stent graft to the aneurysmal site and expanding it to adhere to the arterial wall to reduce the aneurysm to the inside of the stent graft.

Aneurysm ruptures under the influence of various factors such as size, diameter and hemodynamic forces[6,7]. Although the maximum diameter of aneurysm is considered to be a significant factor in rupture[6], the arterial wall stress may better predict the rupture potential of AAA relative to the size and diameter of aneurysm. The rupture of the AAA occurs when the wall stress caused by the blood flow exceeds the aneurysmal wall strength. Therefore, the wall stress as von Mises stress acting on the arterial wall is an important factor for AAA rupture and the numerical analysis is mainly applied to evaluate this mechanical parameter to predict the rupture potential of AAA. Raghavan *et al*.[8,9] has reported that the failure stress of AAA varies from 0.34 to 2.4MPa in the region of aneurysmal surface.

A complicated morphological aneurysm, such as a short aortic angular neck or highly proximal angulated neck, causes a complex pattern of blood flow in AAA[10]. To investigate blood flow behavior through the angular AAA neck inlet angulation we generate the idealized AAA models.

The aims of mathematical modeling of aneurysm in this study are to lead the understanding of pathogenesis of the disease and to improve the criteria for the prediction of rupture risk. Therefore in this study, FSI simulations were performed to investigate the effect of neck angular variation on the rupture risk of AAA. Aneurysm growth is likely to occur in regions exposed to abnormally high or low wall shear stresses (WSS). Although the effect of WSS on the expansion of an aneurysm is not well understood, high WSS is associated with the initiation of aneurysm, and low WSS is related to aneurysm progression, thrombus formation as well as its rupture. Thus the understanding of the processes for the growth and structural weakening of AAA using fluid-structure interaction (FSI) is necessary for the diagnosis of the lesion progression and the design of the patient-specific intervention.

FORMULATION OF THE PROBLEM

Geometric Model of Abdominal Aortic Aneurysm

In this study the three-dimensional AAA geometries were constructed by using Computer Aided Three-Dimensional Interactive Application (CATIA, v5) provided by Dassault Systemes. The idealized AAA geometrical models are shown in Fig. 2(a) and the dimensions of geometry are presented in Table 1. The thickness of the vessel wall is 2mm and the neck angulation α varies from 0^o to 20^o.

Table 1. Dimensions of AAA geometries to be simulated

Geometries	Dimension (mm)
Inlet diameter (d)	20
Outlet diameter of iliac artery (d_1)	12
Outlet diameter of renal artery (d_2)	6
Diameter of aneurysm (D)	50 or 60
Length of AAA (L)	128.6
Length of iliac artery from branch of AA (L_1)	67
Length of renal artery from axis AA (L_2)	40
Neck angle (a)	0, 10, 20
Branch angle (b)	60 or 80
Vessel wall thickness (t)	2

The parametric study in AAA models is carried out examining effects of the possible risk factors of rupture. The FSI simulations are conducted to analyze the impact of the geometrical shapes such as aneurysm size and neck angle in the aorta proximal the aneurysm bulge.

Flow Modeling

We consider viscous flow in a compliant vessel simulating blood flow in stenotic arteries. The blood is assumed to be incompressible, laminar and Newtonian, while the wall is isotropic and elastic.

The governing equations for the conservation of mass and momentum of an incompressible and Newtonian fluid are the axisymmetric, time-dependent Navier-Stokes equations, which are shown as follows:

- Continuity equation

$$\nabla \cdot \vec{U} = 0 \text{ ---------- (1)}$$

- Momentum equation

$$\frac{\partial \vec{U}}{\partial t} + (\vec{U} \cdot \nabla \vec{U}) = -\frac{1}{\rho}\nabla P + \upsilon \nabla^2 \vec{U} \text{ ---------- (2)}$$

where $\vec{U}$ are the velocity vector of the blood velocities, ρ is the blood density, ρ= 1,050 (kg/m^3), and ν is the kinematic viscosity, 3.33x10^{-6} (m^2/s).

The stress tensor in the Cartesian tensor notation is defined below: $\sigma_{ij} = -p\delta_{ij} + \tau_{ij}$

$$\tau_{ij} = 2\mu\varepsilon_{ij} \text{ ---------- (3)}$$

where δ_{ij} is the Kronecker delta, τ_{ij} are the components of the shear stress tensor, $\varepsilon_{ij} = \frac{1}{2}\left(\frac{\partial u_i}{\partial x_j} + \frac{\partial u_j}{\partial x_i}\right)$ are the components of rate of deformation tensor, μ is the dynamic viscosity of the fluid and *i, j* represent the axial and radial direction, respectively.

Wall Modeling

The stenotic wall is considered to be isotropic and elastic with Young's modulus E=2.7×10^6 (N/m^2), Poisson's ratio ν = 0.45 and density of blood vessel wall ρ_s = 1,200 (kg/m^3). The blood vessel wall thickness is uniform at 2mm in normal region.

The motion of an elastic vessel wall is mathematically described by the equation shown below:

$$\rho_s \frac{\partial^2 d_i}{\partial t^2} = \frac{\partial \sigma_{ij}}{\partial x_j}, \text{ for } i, j=\text{x, r} \text{ ---------- (4)}$$

where ρ_s is the vessel wall density, d_i are the components of the wall displacements and σ_{ij} are the components of the wall stress tensor. The stress tensor σ_{ij} is obtained from the constitutive equation of the material, and it can be expressed for a Hookean elastic wall as:

$$\sigma_{ij} = \lambda_L e_{kk}\delta_{ij} + 2\mu_L e_{ij} \text{ ---------- (5)}$$

where λ_L and μ_L ate the Lame constants and e_{ij} are the components of the strain tensor in the solid.

The conditions of displacement compatibility and traction equilibrium along the fluid-structure interface are satisfied:

- Displacement Compatibility

$$\vec{d}_f = \vec{d}_s \text{ ---------- (6)}$$

- Traction Equilibrium

$$\vec{f}_f = \vec{f}_s \text{ ---------- (7)}$$

where $\vec{d}$ and $\vec{f}$ are displacement and tractions and the subscripts *f* and *s* stand for fluid and solid respectively.

Boundary Conditions and Numerical Method

The governing equations were solved using finite element commercial computational fluid dynamic software ADINA (version 9.3, ADINA, Watertown, MA). ADINA fluid-structure interaction code is developed to apply for fully coupled analysis of fluid flow with structural interaction problem. To solve the fluid equations coupled with solid equations ADINA is employed in this study. Time dependent flow waveform[7] was applied at the inlet of the geometry (see Fig. 1) and zero pressure condition was assumed at the outlet region. A no-slip condition at the fluid-solid interface was applied.

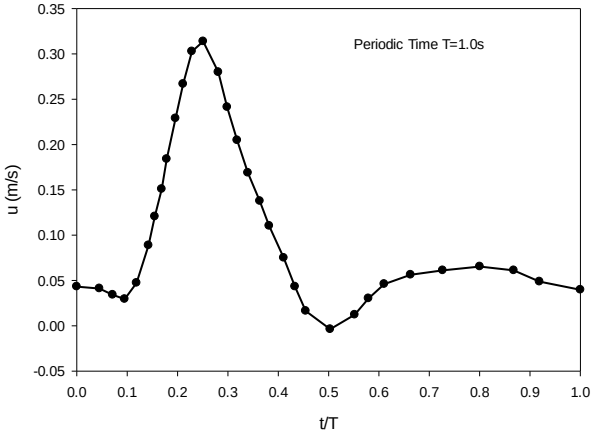

Figure 1. Time dependent inlet flow waveform

Fluid flow was solved by applying the direct solution method with applied 0.8 relaxing force and displacement. Meshing was composed of Rule-Based meshing method which is a Structural Meshing Algorithm. Four node tetrahedral FBCI (Flow Based Control Interpolation) elements were used in fluid domain. Simulation results were assumed to be independent of the computational mesh when the disparity between meshes of varying densities was less than 5%. The Newton Method has been adopted as the iterative algorithm in all simulations. Maximum iteration repeated 15 times in order to in one step and allowable error was 10^{-3}. Time periodic solutions were typically obtained after 4 cycles and were defined when the cycle average difference in the size of the recirculation zone in the vicinity of the stenotic region fell below 5%. All the computations were performed using 2.9GHz Intel Xeon ® CPU E5-2667 (64GB of RAM) personal computer running Windows 7.

RESULTS AND DISCUSSION

Characteristics of Velocity Profiles and Pressure Distributions

Figs. 2 represent the schematic diagrams and the velocity distributions at diastole period for model cases. The neck angle is 0º, 10º, and 20º for cases 1, 2 and 3, respectively. The flow entering into the aneurysm from the inlet region impinges into the lateral wall due to the neck angulation. Therefore the flow distributions are skewed toward the lateral wall. As the neck angulation increases, it can be seen the region of the lateral side along the proximal axis is gathering more and more blood flow while the opposite region is gradually decreasing the flow to form a large vortex. Therefore it can be seen that the region formed a large vortices is almost empty space with no blood flow, as shown in Fig. 2(d).

a) Geometric models b) Velocity distribution at diastole in case 1 c) Velocity distribution at diastole in case 2 d) Velocity distribution at diastole in case 3

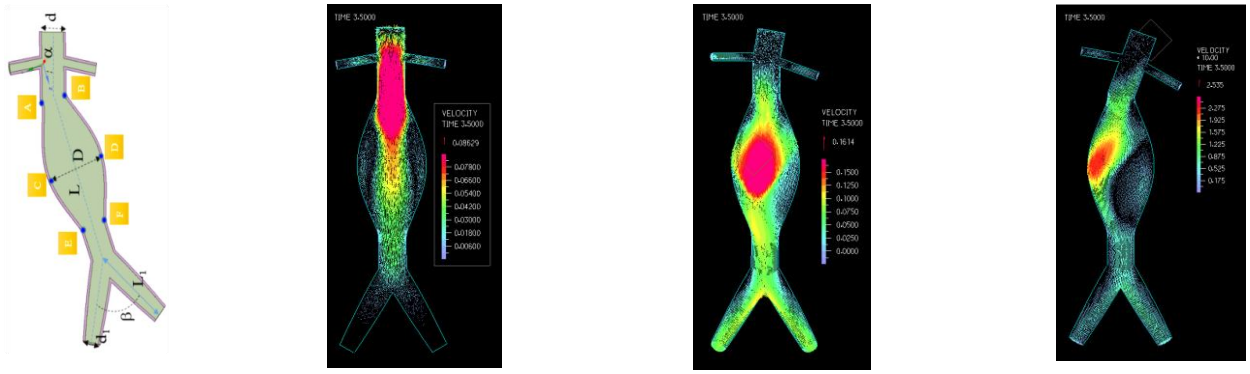

Figure 2. Schematic diagrams and the velocity distributions at diastole for model cases

Figs. 3 illustrated the pressure distributions at the points C and D in Fig. 2(a) as shown during the cardiac cycle for model cases. As the neck angulation increases, the pressure distributions at points C and D can be seen to vary significantly. However, it can be seen that the pressure distribution at the points C and D is almost similar in Fig. 3(a) and (b) when the neck angulation is zero. Considering the results of the velocity distribution in Fig. 2(b), it can be seen that the blood flow distribution is symmetrically distributed, which is related to the pressure distribution. However, as the neck angulation increases, the velocity distributions of model case 2 and 3 are shown to be asymmetric, unlike model case 1 as shown in Fig. 2. As a result, the pressure at point C decreases during the decelerating phase in Fig. 3(a), but the pressure at point D increases inversely.

a) b)

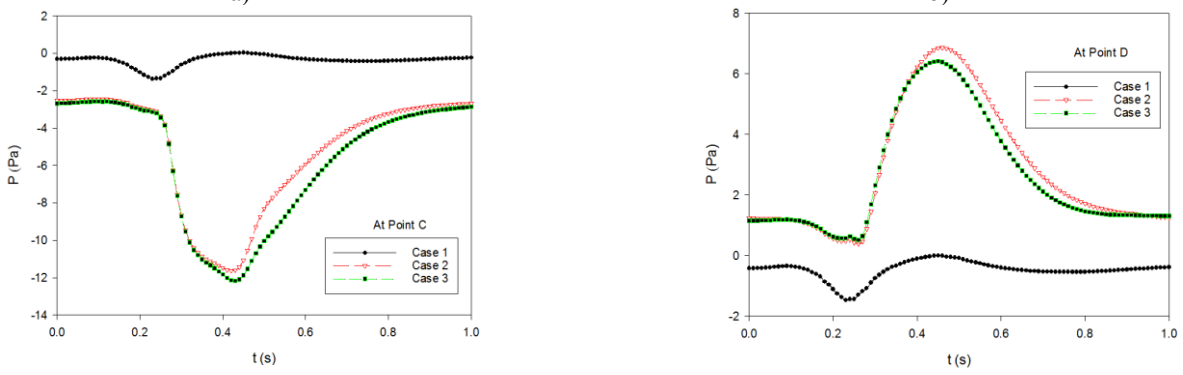

Figure 3. Pressure distributions at the points of maximum diameter of AAA for model cases

Characteristics of Wall Stress Distributions

Figs. 4 represent the shear stress distributions at points C and D for model cases and at six different points for model case 3 during the cardiac cycle. As shown in Fig. 4(a), the shear stress pattern at point C in model case 1 is similar as the inlet velocity pattern of the blood flow (see Fig. 1). However, in model cases 2 and 3, the shear stress increases significantly when the blood velocity is minimum. The magnitude of shear stress at the peak systole is less than o.1Pa in both model cases 2 and 3.

a) Shear stress at point C b) Shear stress at point D c) Shear Stress for case 3

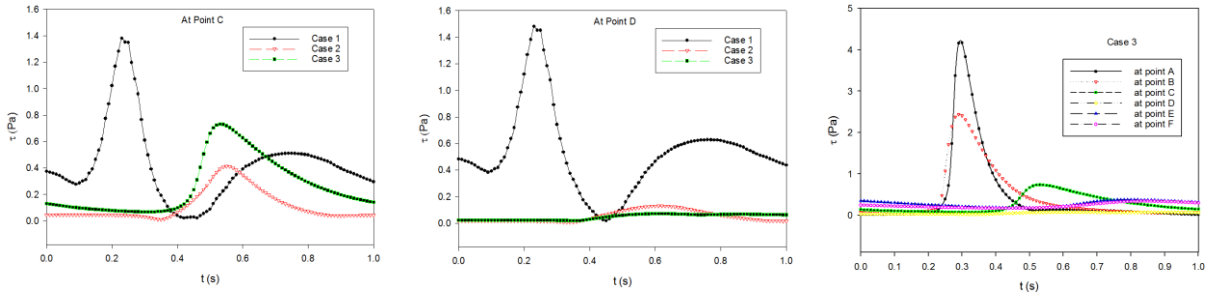

Figure 4. Shear stress distributions at points C and D for model cases and at 6 different points for case 3 during the one cardiac cycle

Figs. 5 show the Von Mises stress distributions at points A and D for model cases and at six different points for model case 3 during the cardiac cycle. The peak Von Mises stresses at points A and D increase as the neck angulation increases, as shown in Fig. 5(a) and (b). As shown in Fig. 5(c), Von Mises stresses are most pronounced at points A and B during the decelerating phase in the cardiac cycle where the blood vessel is bent. These results suggest that AAA are more likely to rupture in the neck regions.

a) Von Mises stress at point A b) Von Mises stress at point D c) Von Mises Stress for case 3

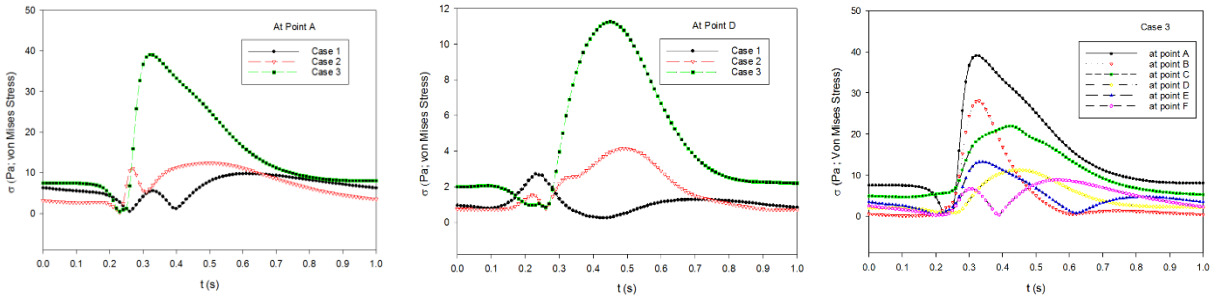

Figure 5. Von Mises stress distributions at points B and D for model cases and at 6 different points for case 3 during the one cardiac cycle

Characteristics of Wall Displacement

Figs. 6 show the characteristics of wall displacement at points A and C for model cases and at six different points for model case 3 during the cardiac cycle. During the accelerating phase in cardiac cycle of blood flow, the displacement at point A increases as the neck angulation increases. Comparisons of the wall displacements among the model cases show that the maximum wall displacement occurred in model case 3. The largest wall displacement was at point A among 6 different points in model case 3 as shown in Fig. 6(c). Wall displacement was higher and longer as the neck angulation is larger, and this can effect on AAA, moreover, could collapse it.[11]

a) Displacement at point A b) Displacement at point C c) Displacement for case 3

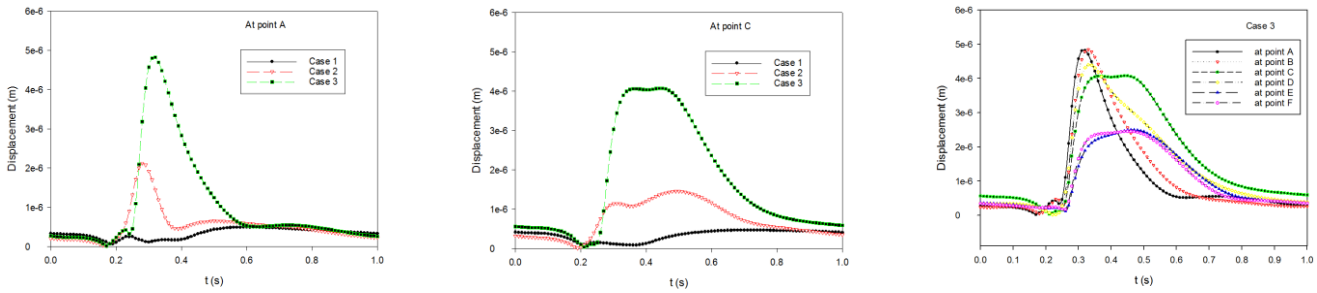

Figure 6. Shear stress distributions at points C and D for model cases and at 6 different points for case 3 during the one cardiac cycle

CONCLUDING REMARKS

In this research, FSI simulation was accomplished under the physiological flow condition cases with time variation for three model cases by using commercial CFD code, ADINA 9.3 (Watertown, MA, USA)[13].

The fluid dynamics and vessel mechanical behaviors were found to be an axisymmetric from the results for flow velocity, wall displacement and Von Mises stress. The effects of FSI model case 1 under the physiological flow condition did not change the fluid and solid behaviors significantly. However, in model cases 2 and 3, the effects of the angulation factor were higher which blood flow could be closure or vessel wall could be collapsed because of high angulation and high stress.

Von Mises stress was higher at higher neck angulation. According to clinical point, hemodynamic factors play an important role on the AAA rupture. As the neck angulation increases, the Von Mises stress increases and the possibility of rupture increases. In particular, the Von Mises stress at point A in the proximal site is the highest and the possibility of rupture is predicted here.

ACKNOWLEDGMENT

This work was supported by the Andong National University research fund in year 2017.

REFERENCES

[1] Maier A, Gee MW, Reeps C, Pongratz J, Eckstein HH, Wall WA. A comparison of diameter, wall stress, and rupture potential index for abdominal aortic aneurysm rupture risk prediction. *Ann Biomed Eng*. 2010;38:3124-3134.

[2] Sarac TP, Bannazadeh M, Rowan AF, Bena J, Srivastava S, Eagleton M, et al. Comparative predictors of mortality for endovascular and open repair of ruptured infrarenal abdominal aortic aneurysms. *Ann Vasc. Surg*. 2011;25:461-468.

[3] Elger DF, Blackketter DM, Budwig RS, Johansen KH. The influence of shape on the stresses in model abdominal aortic aneurysms. *J Biomech. Eng*. 1996 Aug; 118 (3) :326-32.

[4] Volokh KY. Comparison of biomechanical failure criteria for abdominal aortic aneurysm. *J Biomech*. 2010 Jul 20; 43 (10) :2032-4.

[5] Patel V. Impact of geometry on blood flow patterns in abdominal aortic aneurysms. Master thesis, 2011.

[6] C.M. Scotti, J. Jimenez, S.C. Muluk and E.A. Finol, Wall stress and flow dynamics in abdominal aortic aneurysms: finite element analysis vs. fluid-structure interaction. *Computer Methods in Biomechanics and Biomedical Eng.* 2008 June;11(3):301-322.

[7] P. Rissland, Y. Alemu, S. Einav, J. Ricotta and D. Bluestein, Abdominal aortic aneurysm risk of rupture: Patient-specific FSI simulations using anisotropic model. *J. Biomech. Eng.* 2009 March;131

[8] M.L. Raghavan, J. Kratzberg, E.M. Castro de Tolosa, M.M. Hanasoka, P. Walker and E.S. de Silva, Regional distribution of wall thickness and failure properties of human abdominal aortic aneurysm. *J. Biomech*. 2006;39(16):3010-3016.

[9] Y. Mesri, H. Niazmand, A. Deyranlou and M.R. Sadeghi, Fluid-structure interaction in abdominal aortic aneurysms: structural and geometrical considerations. *Int. J. Modern Phys C*. 2015;26(4):1550038(18pages).

[10] Y.A. Algabri, S. Rookkapan and S. Chatpun, Three-dimensional finite volume modelling of blood flow simulated angular neck abdominal aortic aneurysm. *IOP Conf. Series: Materials Science and Engineering.* 2017:243

[12] Fry, D. L., Acute vascular endothelial changed associated with increased blood velocity gradients, *Circ. Res.* 1968;22: 165-197

[13] http://www.adina.com/